Soil variability mapping with airborne gamma-rays spectrometry and magnetics

L. Ameglio[1], E. Stettler[2] and D. Eberle[2]

1. EXIGE Pty. Ltd., South Africa and Australia, laurent@exigesa.com
2. AeroPhysX Pty. Ltd., South Africa

A paper from the Proceedings of the
15th International Conference on Precision Agriculture
June 26-29, 2022
Minneapolis, Minnesota, United States

Abstract. Over the past 50 years airborne geophysics has become an effective and standard technology in mining and minerals exploration programs for mapping various signatures on the Earth's surface and at depth. In this paper we present the potential of such approach to digital soil mapping too. A trial airborne gamma-ray spectrometric (4ltr CsI crystal system) and magnetic (fluxgate sensors) survey was conducted over a farm land (~ 153 ha) in South Africa. The survey was flown with an affordable gyrocopter at 20 m agl, 20 m line spacing and at an averaged 100 km/hr speed. A total of ~ 67,000 airborne measurement points were collected in less than 2 hours work as opposed to weeks of work for a ground-based soil sampling program. The airborne survey provides a resolution of ~ 438 points/ha, more than 400 time higher than that of the soil sampling program at ~ 1 points/ha.

Separating the magnetic field solely due to the soil from the underlying rock(s) proved difficult as expected. The calculated soil magnetic susceptibility from the airborne data was hence not useful for digital soil mapping. This aspect requires further investigation including possible alternative ways to determine soil magnetic susceptibility through for example the use of both electromagnetic and magnetic techniques.

Airborne gamma-rays mapping proves to be powerful in mapping the content and spatial variability of soil potassium (eK), uranium (eU) and thorium (eTh). It also proves successful in

predicting soil sand (with gamma-rays Total Count as proxy) and clay (with eTh as proxy) contents. The gamma-rays classic manual data interpretation allowed to identify four main soil zones instead of only two zones from the ground grid work. Further manipulation of the airborne geophysical data using an integrated approach based on multivariate statistical analysis tools (cluster analyses) enabled data-driven, automated, and rapid data integration for digital soil map generation.
Finally, airborne survey ancillary information about soil elevations (0.5 to sub-m in x and y and 10-25 cm in z) and environmental characteristic (dose rate) also proves to be critical information for decision making with farm land management aspects.

Keywords. Airborne geophysics, gamma-ray spectrometry, magnetics, digital soil mapping, precision agriculture, soil variability, soil zoning, environmental, elevation, data fusion.

Introduction

Mapping the spatial distribution of the physical and chemical properties of agricultural soils is critical for profitable and sustainable crop and food production. The measurement of such soil properties presents however obvious problems arising from sampling a dense, opaque and very heterogeneous medium. Conventional methods consisting of ground-based grid surveying are laborious, expensive and lack appropriate spatial resolution to allow best farm management decision in precision agriculture. Over the past 50 years, airborne geophysics using conventional aircraft has however become an effective and standard technology in mining and mineral exploration programs for mapping various signatures on the Earth's surface and at depth (Horsfall, 1997). The last decade, Light Sport Aircraft (LSA) have also matured into operational tools providing new horizons compared to conventional aircraft, with lower capital outlay and operational cost as added values (Ameglio *et al.*, 2018, Bongartz *et al.*, 2015). Agricultural soil mapping can now also benefit from the powerful information and knowledge encapsulated into standard airborne magnetics and gamma-ray spectrometric data. We demonstrate that approach through a trial survey performed over a crop farming land in South Africa (Ameglio *et al.*, 2018).

Principles of airborne gamma-rays and magnetics surveying

The only way geologists or soil scientists can 'see' below the surface of the Earth without drilling or digging is by making use of geophysics. Geophysicists are like the radiologists in the medical profession. Before invasive surgery, a patient undergoes X-ray, gamma-ray, CAT scans, or electro-scans. The geophysicist performs the same duty on the Earth, thereby reducing the risk of placing a borehole or a dig in the wrong location, or help decision making for Earth surface monitoring and management. Two of the standard geophysical technologies systematically applied to natural resources exploration program nowadays are gamma-rays spectrometry and magnetics. Those methods, and particularly their airborne application for natural resources exploration (Horsfall, 1997), are now briefly introduced within the perspective of their application to agricultural soil mapping.

Airborne gamma-ray spectrometry for non-geophysicists

Gamma-rays are high-energy electromagnetic radiation due to the decay of radio-elements. In everyday life, controlled gamma-rays radiation is used in hospitals to kill cancerous cells ('radiotherapy'). In the nature, gamma-rays can be emitted by neutron stars, pulsars, supernova explosions, and also regions around black holes. It is also regularly emitted by the Earth's surface (albeit weakly and harmless to life forms). Radioactive source elements indeed occur naturally in the crystals of particular minerals in soil horizons and regolith that are the products of various geo-processes (weathering, *etc*) of the underlying bedrock (see Fig. 1). The abundance of minerals changes across the surface of a farm land with the lateral variations at depth of the bedrock and regolith types. Because the energy of gamma-rays is related to minute amounts of radioactive source elements (*i.e.* Thorium, Uranium and Potassium), gamma-rays can then be used to measure the abundance of those elements in a soil. So, by measuring the energy of gamma-rays being emitted by farm land, we can infer the presence of particular minerals in that farm land surface soil and characterize the ground spatial variability of soils.

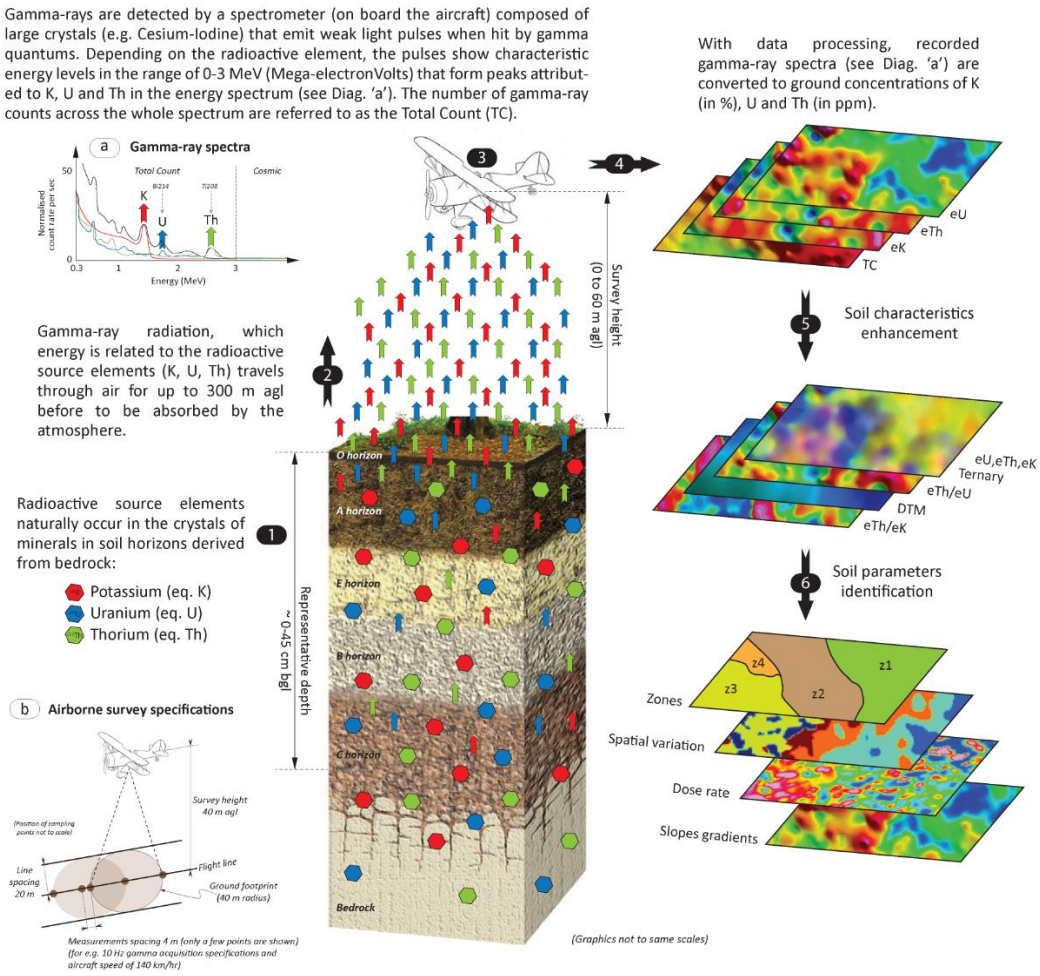

Fig. 1. Principle of airborne gamma-ray spectrometry for agricultural soil imaging.

Gamma-ray spectrometry presents however a certain number of limitations such as:

- ✓ after numerous corrections (step 4 in Fig. 1) it reflects the equivalent Potassium (eK), Uranium (eU), and Thorium (eTh) concentrations at surface (IAEA, 2003), equivalent indicated by the 'e'. The concentrations are called 'equivalent' because they don't stem from a chemical analysis from a soil/rock sample determined in a laboratory.
- ✓ it has virtually no depth penetration. If the geology is sub-outcropping, then the radioelement concentrations can be used to differentiate between different types of geology and gamma-rays spectrometry complements geological maps and drainage patterns well. The Total Count (TC) map is frequently very useful to locate outcrops and to give a general overview of the geology.
- ✓ the 'footprint' of an airborne gamma-rays spectrometry (Fig. 1, diagram 'b') is the minimum ground surface of investigation contributing to the detected/measured radiation by the spectrometer in the aircraft at its survey heights (IAEA, 1991). As a rule of thumb, 66% of the counts originate from an area covering twice the altitude width and twice the altitude plus the forward movement distance length (Ward, 1981).
- ✓ A hindrance in gamma-ray spectrometry is the effect of water logging and also moisture in soil where 40 cm of moist soil will attenuate approximately 90% of the gamma radiation emanating from that soil (Beamish, 2013).

A comprehensive critical review of gamma-ray spectrometry (not only its airborne application)

used as a tool in soil sciences is also presented by Reinhardt and Hermann (2019).

Airborne magnetics for non-geophysicists

The spatial configuration of the soil and its underlying rocks (including fault affecting soil horizons) produces a local magnetic field (grey lines in Fig. 2, step 1) whose directions and magnitudes at the surface add up to those of the Earth's main magnetic field (Fig. 2, diag. 'a') which over a small area is close to uniform (dashed line and black arrows in Fig 2, step 1). The resulting field is called the Total Magnetic field Intensity (TMI). As the aircraft flies along a set of parallel lines (Fig. 2, step 2) covering the survey area, the magnetometer(s) on board measures and records the TMI at the sensor(s) position (usually at the wings tips or on lateral and/or tail booms). The measured TMI is the sum of: (i) the Earth main magnetic field; (ii) tiny temporal variations (diurnal effect); (iii) solar wind effects; (iv) the magnetic field of the survey aircraft itself; and finally (v) the much-wanted magnetic signal of the targeted geological information (rocks units, faults, soil). By subtracting/correcting for effects (i) to (iv), the resulting aeromagnetic map (see Fig 2, step 3, top map) shows the spatial distribution and relative abundance of magnetic minerals at ground level. Different rock types and geological structures differ in their content of magnetic minerals allowing their visualization in sub-surface in the form of hills, ridges and valley referred to as magnetic anomalies (Fig. 2, diag. 'c'). Further data enhancing and modelling can then infer shape, depth and properties of the rock units and/or geological structures responsible for those magnetic anomalies (Fig. 2, steps 4 and 5).

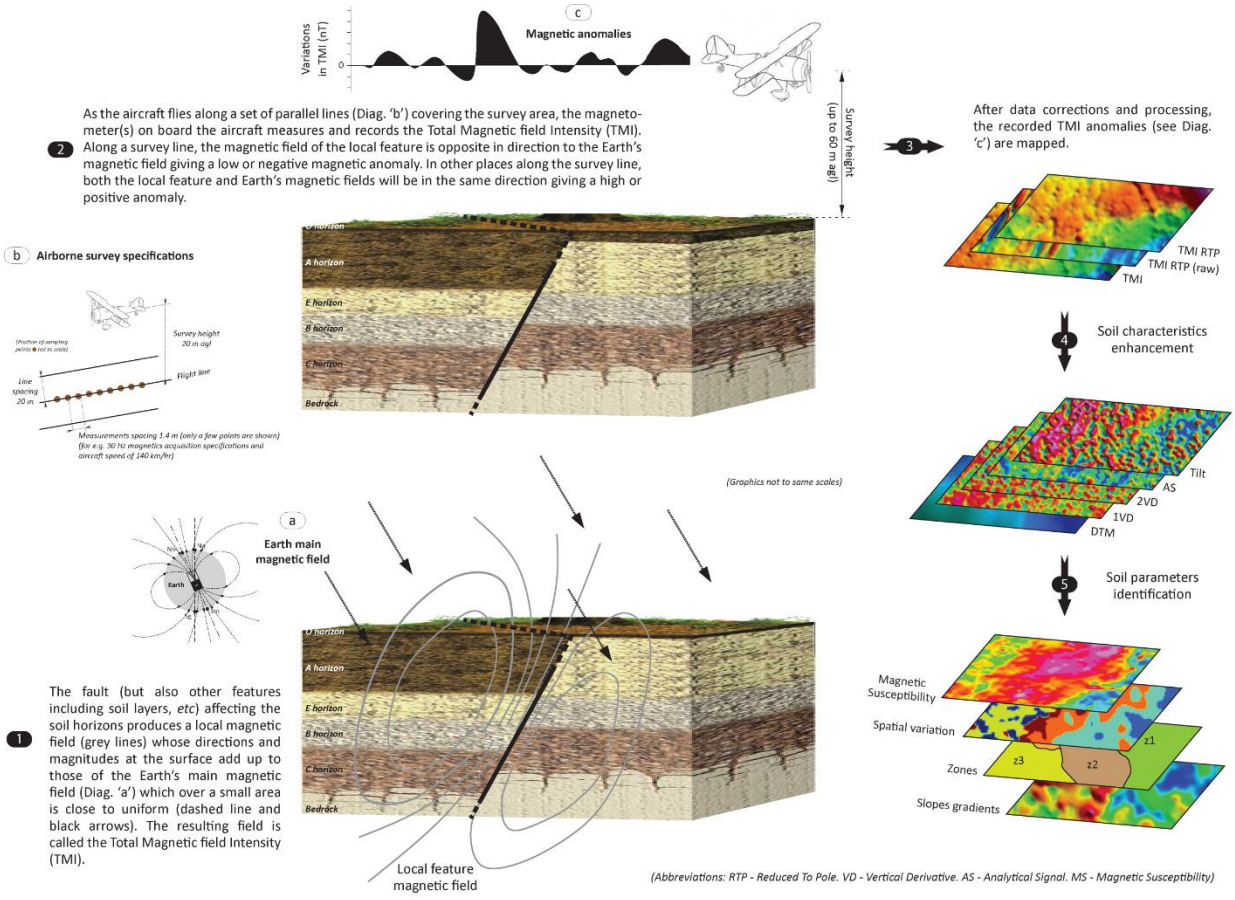

Fig. 2. Principle of airborne magnetic for agricultural soil imaging.

Airborne gamma-rays and magnetics survey results

Airborne survey technical specifications

An experimental low-level flying height airborne magnetic and gamma-rays spectrometry survey was flown over a farm land (~ 153 ha) in the North-West region of South Africa (Fig. 3). The survey was flown on board a gyrocopter (Fig. 3a) at 20 m agl (above ground level), 20 m line spacing (see flight path in Fig. 3b, white lines) and at an average speed of ~ 100 km/hr speed. A total of ~ 67,000 measurements points were collected in less a than 2 hours work and providing a resolution of 438 point/ha. The acquired data was corrected and processed (see apercu in Horsfall, 1997) and both magnetic and gamma-rays anomalies acquired were interpreted.

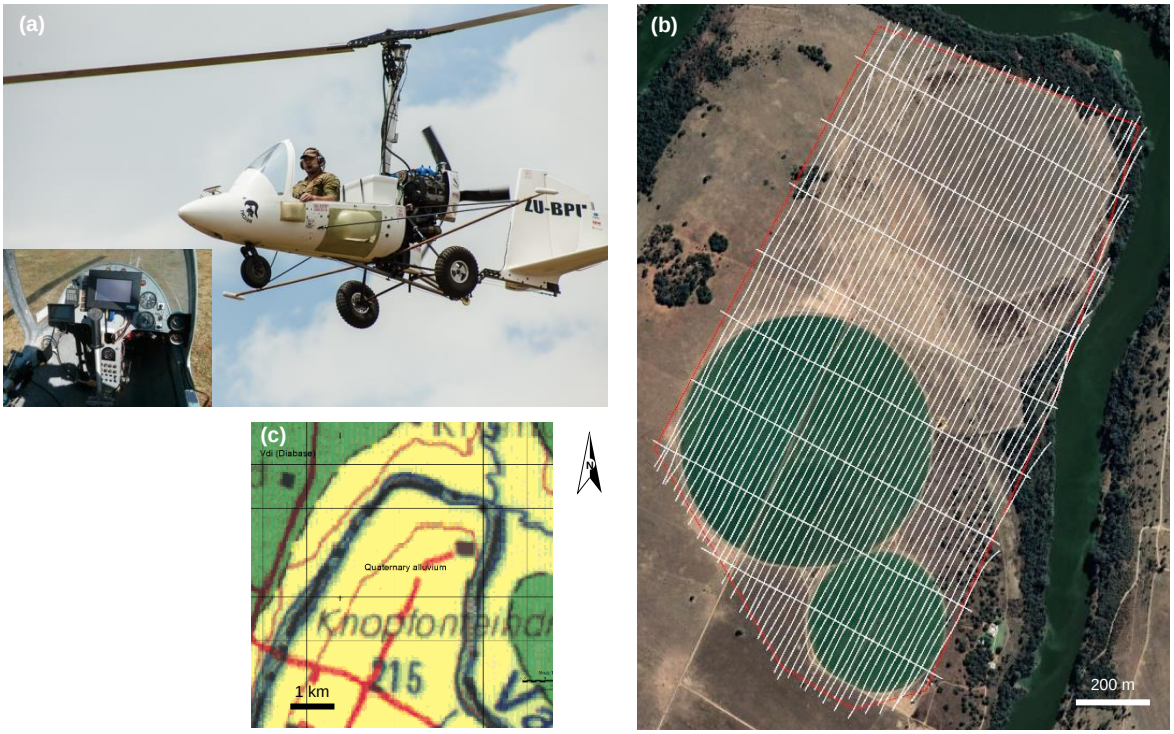

Fig. 3. (a) GyroLAG Pty Ltd modified gyroplane with horizontal gradient fluxgate magnetic system (collaboration with UNISTRA, France) and CsI 4 ltr crystal spectrometer. Inset: cockpit view with navigation computer (center) and data acquisition pilot display (left). (b) Flight path (white lines) within the boundary (red outline) of the airborne survey area. (c) Geological context (Council for Geoscience, South Africa) with diabase (green) and quaternary alluvions (yellow).

A cautionary consideration about the actual dimensions of the smallest detectable anomalies is always necessary with geophysical survey. The aircraft survey velocity ranged from 85 to 110 km/h which translates to an average of ~ 27 m/s. The fluxgate magnetometers (Munschy *et al.*, 2006, Ameglio *et al.*, 2015) used to record the magnetic field strength of the Earth sampled at 20 Hz frequency (*i.e.* 20 times a second) equivalent to a reading every ~ 1.3 m. The gamma-ray data was acquired with a 4 ltr Cs-Iodine crystal at 10 Hz equivalent to a reading every ~ 13 m. The Nyquist law applied to physics on what constitutes significant trends in line data, states that at least 3 data points are necessary to identify a trend or an 'anomaly' in a data set (but geophysicists usually prefer 4 or 5 data points to be able to attach statistical significance to an 'anomaly'). The importance of this is that a narrow soil feature of less than ~ 3 m wide is not going to register in the magnetic data set for example. The gridding of data also reduces the high frequency content of the data leading to the over estimation of depth to magnetic rocks. Both limitations are however partly mitigated by the narrower survey line spacing used in the present survey. Then, for the gamma-ray data, one major limiting factor is related to the 'footprint' of the measurement (see previous section of the paper with Fig. 1, diag. 'b'). The above limits are however the state-of-the-art for airborne surveys and can only be improved upon by flying narrower flight line spacing's

(but already tigh on the present survey), and/or flying slower (using a UAV, not necessarily cheaper compared to light sport aircraft like a gyrocopter) and/or sampling faster.

Gamma-ray spectrometry data – Soil zoning and variability

Gamma-ray spectrometry is limited to approximately the first 30-45 cm of the ground surface. As such, it is a very powerful tool for surface soil zooming and variability mapping. Some of the results of the survey are presented in Fig. 4.

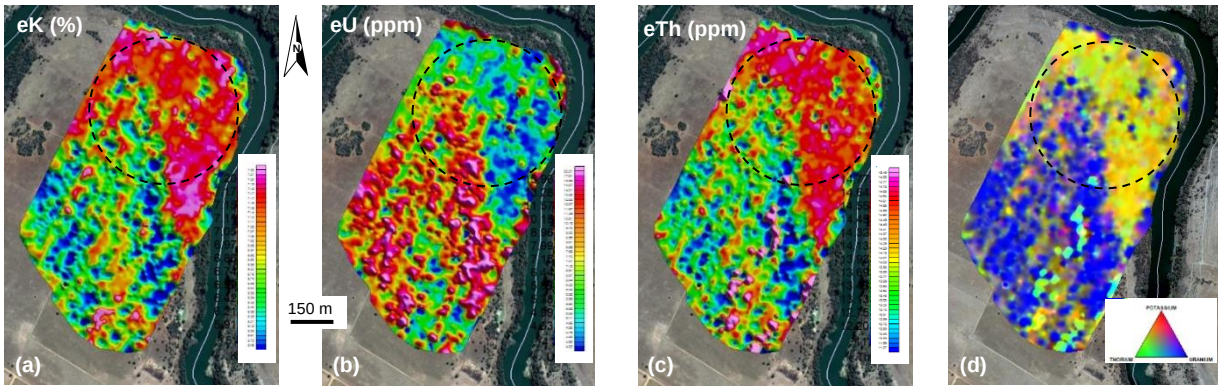

Fig. 4 Soil variability airborne gamma-ray spectrometry mapping. Black dashed line: outline of pivot farming in Fig. 5. All maps at same scale. (a) Potassium (eK) concentration (%). (b) Uranium (eU) concertation (ppm). (c) Thorium (eTh) concentration (ppm). (d) Ternary plot of K, eU and eTh. See also Fig. 6 for the magnetic data flown over the same area at the same time than gamma-ray spectrometry.

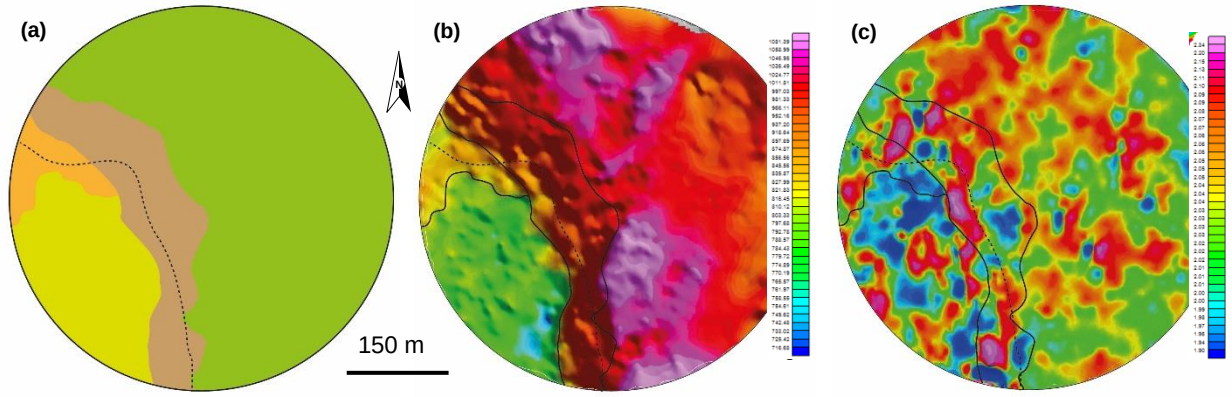

Fig. 5. Soil zones identification and lateral variability over the northern farming pivot of the survey area. (a) Four soil zones are identified with airborne data (mainly eK, eTh, eU, Total Count and various ratios such as eTh/eK and eK/eU). The dotted line separates the only two soil zones identified by ground investigation. (b) Airborne gamma-rays spectrometry Total Count map. (c) Airborne gamma-rays spectrometry eTh/eK ratio distribution. Soil zones limits of Fig. 5a also overlaid on Fig. 5b and c (solid lines - airborne soil zones; dotted line - ground soil zones). All maps at same scale.

The soil survey ground investigation (Dreyer and Ameglio, 2018) of the northern pivot (dashed line circle in Fig. 4a) revealed two distinct soil types/bodies. Along the river the parent material is alluvium with an average silt and clay content of 28%. Further away from the river the soil is deep eolian sand with less than 10% silt and clay content. The limit between those two soil zones is represented in Fig. 5a (dotted line). The gamma-rays Total Count map (Fig. 5b) also identifies two major soil zones in the airborne data. One soil zone, S-SW of the pivot, is depleted in eK and eTh and richer in eU and corresponds to gravel/sandy soil. The other soil zone, N-NE of the pivot, is rich in eK and eTh and corresponds to a clayish soil. The ternary plot of eK, eTh and eU (Fig. 4d) shows that both zones also display a substantial degree of lateral variability of the soil which is not fully imaged on the single radio-elements maps (Fig. 4a to c). This high variability is further enhanced in the map of eTh over eK (Fig. 5c). Analysis of all of the airborne data over that pivot (potassium, uranium, thorium - Fig. 4a to c - but also ratios of those elements) allow to however

identify four main soil zones (Fig. 5a) instead of the two zones from the ground grid work.

Magnetic data – Soil magnetic variability and magnetic susceptibility

Magnetic imaging is a more complex affair than gamma-rays spectrometry imaging for surface soil zoning and variability mapping. This is due to the fact that the magnetic signal: (i) can be severely impacted by surface and sub-surface human artifacts (or anthropogenic noise); and (ii) incorporates the effect of multiple sources at various depth of the Earth down to several kilometers (see Fig. 2 and associated text).

With respect to anthropogenic noise, Fig. 6a (southern pivot - dashed white outline) clearly shows the magnetic signal of the metal spraying system in the western half of the pivot. Also in Fig. 6a (but northern pivot - dashed black outline), that very strong (pink hues) NW-SE elongated magnetic feature is the magnetic signature of an underground drain and/or water pipeline feeding that pivot. The position of that underground pipeline is also marked as a gutter-like feature (blue hues) in the aircraft laser altimeter topographic map (Fig. 6c) where the land must have also been terraformed. Most of those human artifacts can however be removed (mainly by manual processing) from the airborne dataset as shown when comparing Fig. 6a and b for the southern dashed white outlined pivot.

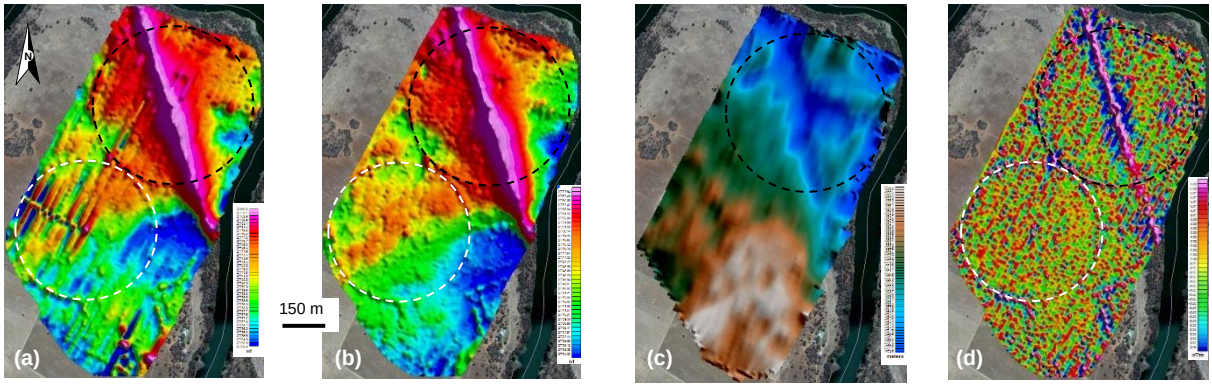

Fig. 6. Soil airborne magnetic mapping. Black and white dashed circles outline different pivot farming lands discussed in the text. (a) Total Magnetic Field Reduced To the Pole (TMF RTP) with anthropogenic noise (see text). (b) TMF RTP with most anthropogenic noise removed (except in northern pivot – see text). (c) Topography map from the aircraft laser altimeter.

The Total Magnetic Field (TMF) data (Fig. 6a) even after most anthropogenic noise was removed (Fig. 6b) still displayed the effect of the pipeline feeding the pivot (see in dashed black outline in Fig 6b). The magnetic susceptibility of the upper soil material was provisionally determined by upward continuing the TMF of Fig 6b by 10 m and then subtracting it from Fig 6b. Resulting TMF is shown in Fig. 7a. Repeating the process again by upward continuing Fig. 7a by 10 m and subtracting it from Fig. 7a changes little has shown in Fig. 7b. The resultant magnetic field in Fig. 7b indeed still displays a strong contribution from the pipeline. Applying an equivalent magnetic susceptibility calculation (Fig. 7c) followed by a directional cosine filter of 160° (MAGMAP in Geosoft Montaj) to remove the pipeline effect subsequently brings the magnetic susceptibility result as shown in Fig. 7d. As can be seen in the map of the magnetic susceptibility in Fig. 7d, the effect of the water pipeline is still visible. Another feature visible (Fig. 7c) are several ‘ring-like’ magnetic features (some concentric but of different diameters). Those are frequently observed around such pivot farm and correspond to stones and boulders accumulated at the edge of the pivot during land works (tiling, *etc*). Finally, looking at the large amplitude and spatial variation of the magnetic susceptibility values in the southern half of Fig. 7c and considering the rather homogeneous magnetic pattern of the same area in Fig. 6d (second vertical derivative calculation - enhancing magnetic features at or very close to surface), it appears that the magnetic

susceptibility in that area is more related to a deeper-seated magnetic source(s).

As can be seen, it is very difficult to separate the magnetic field solely due to the soil from the underlying rock and other influences. This aspect requires further investigation. We are also looking at alternative ways to determine the magnetic susceptibility, perhaps through the use of both electromagnetic and magnetic techniques. Therefore, we don't include for the moment the magnetic susceptibility in the cluster analysis discussed in the next section of this paper.

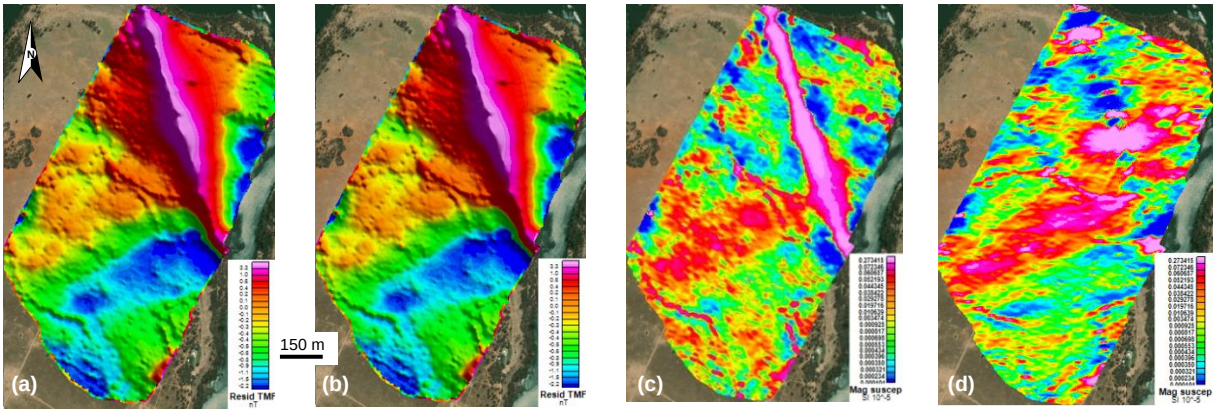

Fig. 7. Soil airborne Magnetic Susceptibility imaging. (a) Residual Total Magnetic Field (TMF) calculated by subtracting 10 m upward continued magnetic field of the measured TMF (see Fig. 6b) from the measured TMF (Fig. 6b). (b) Residual of Residual TMF calculated by subtracting 10 m upward continued magnetic field of the Residual TMF (Fig. 7a) from the Residual TMF (Fig. 7a). Survey area still contains effects from underlying rock and pipeline. (c) Residual of Residual TMF converted to Magnetic Susceptibilities (in SI x 10^{-5}). (d) Magnetic Susceptibilities (in SI x 10^{-5}) with application of a directional cosine filter of 160° to remove pipeline effect. Pipe line effect mostly but not entirely removed but survey area probably still showing influence of deeper rock material.

Fusion of elevation and gamma-ray data – Multivariate soil variability mapping

In mineral exploration or geological mapping, a combination of various geophysical techniques are often used to generate potential exploration targets or make deductions about the geology. Evaluation of the various data sets usually is done successively and results in a manual subjective interpretation of the database. Alternatively, an integrated approach based on multivariate statistical analysis tools, such as cluster analyses, can enable data-driven, automated, and rapid data integration as well as value-added map generation. Clustering (grouping) algorithms can detect several predefined groups in a multimethod database. The detected groups ideally are characterized by little within-group variations, but between-group variations are expected to be significant. Clustering of airborne geophysical data was first presented during the 1980s and 1990s to support geologic mapping (see Paasche & Eberle, 2011 for a history of developments). These studies were initially constrained by poor computer capacity and data quality, but with the advent of more powerful and faster computer facilities, the conditions to apply multivariate statistical analyses in geophysics and remote sensing have improved, thus enabling a varied field of applications.

The result of the clustering process is a classified map. Each class (cluster) is linked to geophysical attributes underlying the clustering procedure. Subsequently, geological attributes are ascribed to each cluster in an interpretational step to obtain a pseudo-lithology map. This concept was proven successful for data-driven and rapid regional-scale mapping (Paasche & Eberle, 2009; Eberle *et al.*, 2010).

Crisp clustering techniques were solely used for the integration of multi-parameter airborne geophysical datasets until Paasche & Eberle (2009) applied the principle of fuzzy partitioning clustering, employing the fuzzy c-means (FCM) algorithm. Crisp cluster algorithms do not provide a quality measure for the classification of each multi-parameter sample. Trustworthiness of cluster

assignment can be obtained from running fuzzy cluster analyses adding value to the visualization of pseudo-lithology maps (Paasche & Eberle, 2009, 2011). Paasche & Eberle (2011) then switched to using the fuzzy Gustafson-Kessel (GK) cluster algorithm (Gustafson & Kessel, 1978) and revisiting the FCM algorithm have proven the results obtained by the GK algorithm to be superior in terms of structural clarity to those obtained by the FCM algorithm.

In the present study, the GK cluster algorithm was used to integrate airborne gamma-ray and topography but not magnetic susceptibility values as the signature is thought to be more linked to material below the soil cover and would contribute very little to the GK clustering used here that concentrates on the surface and very near surface material. The GK algorithm groups n samples located in a t-dimensional space into a specified number of c clusters. For the present case the clustering was unsupervised which means that the result was not steered towards a specific end result. The agreement between the visual derived result (Fig. 5a) and the GK derived product (Fig. 8 – see northern pivot farm) gives therefore confidence in the results. Clustering applied to soil analysis, particularly with airborne dataset, is still in its infancy as many factors can change the outcome and below is just a small sample of some of the clusters obtained. No checks against soil samples have been performed at the time of preparing the present paper.

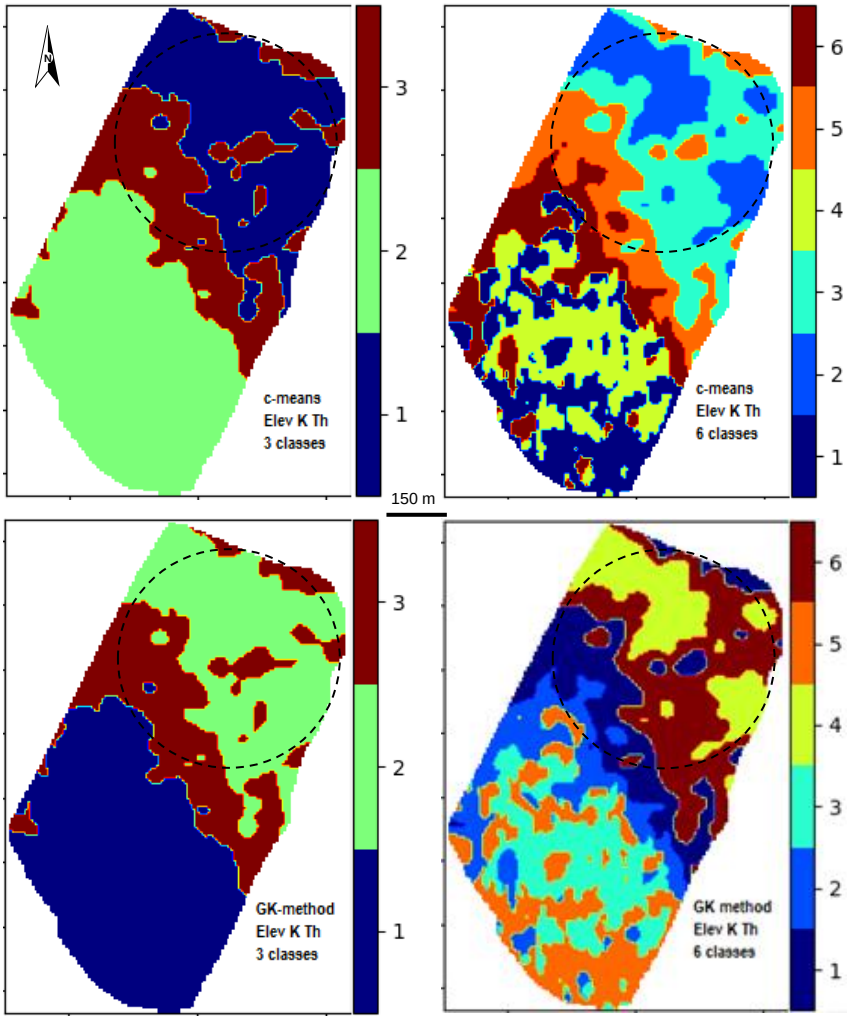

Fig. 8. Soil lateral variability mapping with automatic unsupervised clustering using elevation, eK and Teh datasets. Comparison between the C-means and Gustafson-Kessel (GK) classification (see text for details) identifying 3 and 6 clusters with similar variations in variables elevation, eK and eTh. Black dash line: outline of 800 m diameter pivot.

Discussion

Gamma-ray spectrometry – Proxies for soil clay, sand and K content

Fig. 9 provides a visual comparison of eTh versus soil clay content, Total Count (TC) versus soil sand content and eK versus K measured on soil samples. While comparing those maps it is worth noting: (i) the huge disparity in term of resolution of ground soil samples (1 pt/ha) versus the airborne survey (438 pt/ha); and (ii) some parameters are not expressed in the same unit. Nevertheless, there is a reasonably good agreement between airborne gamma-ray measurements and soil parameters.

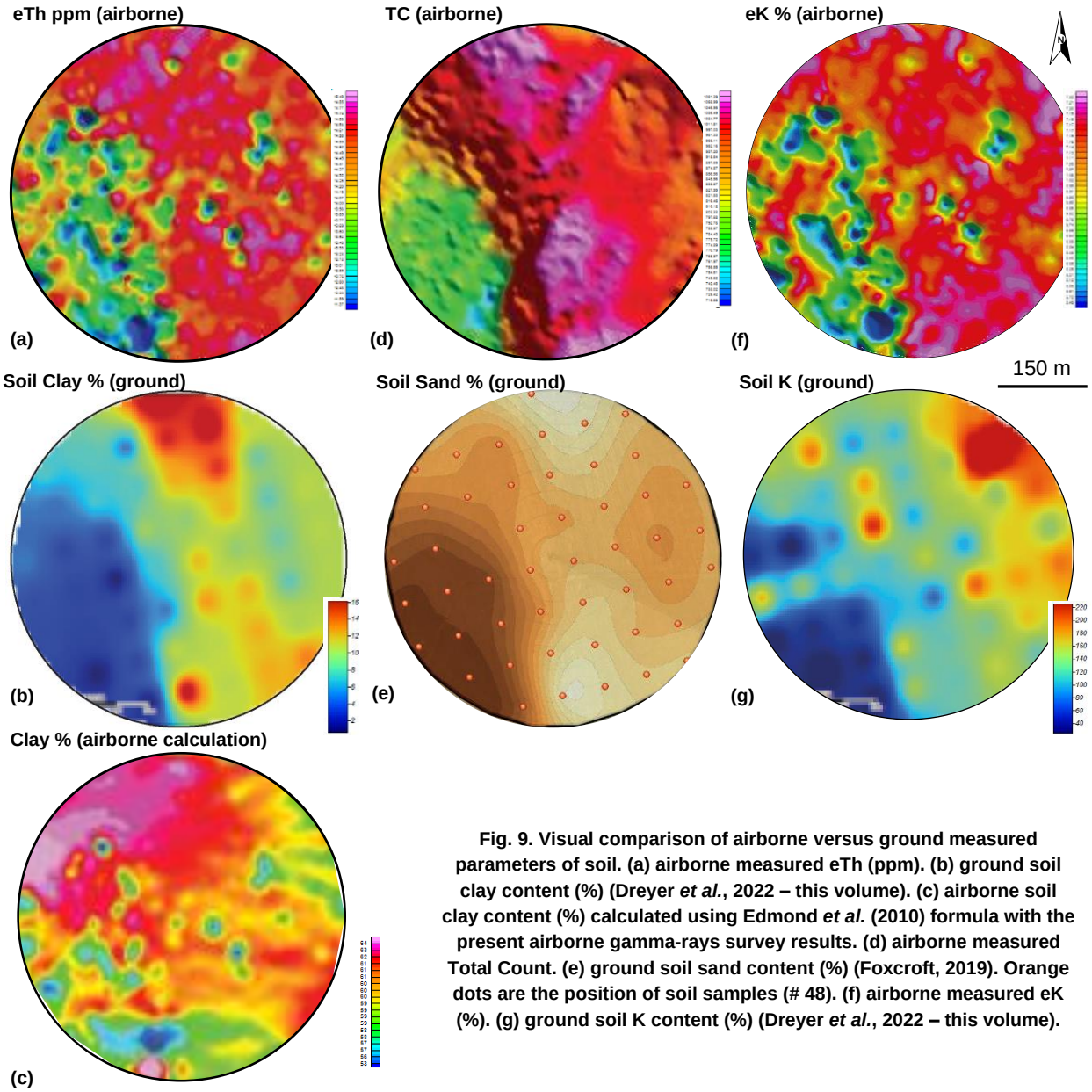

Fig. 9. Visual comparison of airborne versus ground measured parameters of soil. (a) airborne measured eTh (ppm). (b) ground soil clay content (%) (Dreyer *et al.*, 2022 – this volume). (c) airborne soil clay content (%) calculated using Edmond *et al.* (2010) formula with the present airborne gamma-rays survey results. (d) airborne measured Total Count. (e) ground soil sand content (%) (Foxcroft, 2019). Orange dots are the position of soil samples (# 48). (f) airborne measured eK (%). (g) ground soil K content (%) (Dreyer *et al.*, 2022 – this volume).

eTh appears to be a good proxy of soil clay content (Fig. 9a vs. 9b) as already observed elsewhere in the world (*e.g.* Edmond *et al.*, 2010). The work by van Egmond *et al.* (2010) collected soil samples (measuring notably soil clay and Mg content) and ground-based gamma-ray spectrometry ^{232}Th readings on a land of 800 ha (in Netherlands) over three subsequent years. Correlation between the soil samples analyses and gamma-rays spectrometry data provided a good regression equation ($R^2 > 0.7$) between soil clay % and gamma-rays eTh (ppm). The

calculated clay % using Egmond *et al.* (2010) formula and the airborne gamma-ray data of the present study is displayed in Fig. 9c. As it can be seen the results is not in agreement with the measured soil clay content. This illustrate as it would be expected that there can be no linear relationship between the soil encountered in van Egmond *et al.* (2010) case study in the Netherlands and soils elsewhere in the world (here in South Africa). This emphasizes the need for regional calibration of airborne gamma-ray data for fast and efficient automatic extrapolation of thorium concentration airborne map into clay % soil map.

TC is in good agreement (but inverse relationship) with soil sand content (Fig. 9d vs. 9e). Elsewhere in the world (Australia), Taylor *et al.* (2002) found a significant linear relationship (R^2 > 0.71) between clay and TC instead.

Finally, there seem to be a reasonable agreement between eK and soil K content (Fig. 9f vs. 9g). Dreyer *et al.* (2022, these proceedings) has performed an in-depth statistical analysis of the present study's airborne gamma-ray data set and compared it to the soil sample laboratory analyses. They notably show that the airborne gamma-ray data is successful in predicting the soil particle fractions of sand, silt and clay, as well as the soil carbon (C), calcium (Ca) and magnesium (Mg).

Gamma-rays spectrometry – Soil depth, porosity and density estimates

As previously indicated gamma-ray spectrometry has virtually no depth penetration (see Fig. 1). Most of the signal recorded stems from the top 30-45 cm of the ground. Wong *et al.* (2007) however presented a method to estimate soil depth in commonly occurring sandy soil over lateritic cemented gravels/rock landscapes based on attenuation of gamma-ray radiation due to the thickness of the soil layer. The method was tested using both ground and airborne gamma spectrometric surveys coupled with in-situ soil depth measurements. The depth estimates obtained were about 45 cm hence within the range of the physics limitation of the technology and standard gamma-ray data processing methods.

By using non-standard processing method of gamma-ray data through notably the use of ^{214}Bi emissions low energy peaks in the gamma-ray spectrum (see Fig. 1, Diag. 'a'), Beckett (2007, 2008) also showed how soil thickness, but also density and porosity changes in soil/regolith could be established. This approach of using non-standard gamma-ray emissions (*e.g.* also ^{228}Ac or ^{208}TI as per Beckett, 2007) should definitely be the object of further investigations to further enhance the value of airborne gamma-ray spectrometry application to agricultural soil mapping.

Magnetics – Soil erosion index

A detailed field and laboratory study by Nazarok *et al.* (2014) on a small (less than 1 ha) agricultural land in Ukraine demonstrated the applicability of magnetic methods (measuring Magnetic Susceptibility, MS) in soil erosion estimation (in the particular case of strongly magnetic parent material). The study showed that soil MS had a high degree of statistical relationship with erosion index and humus content and MS was used to establish an erosion index of the area. The automatization of such approach to airborne magnetic dataset would allow for a fast and cost-effective assessment of soil erosion level over large surfaces (from individual farm to an entire agricultural region and also at a basin scale). But as shown in the present paper the handling of the magnetic data to calculate MS is not that straightforward and need further investigation.

Hidden information in airborne anscillary data

During an airborne survey a certain number of acquired data (*e.g.* for aircraft navigation purpose), otherwise considered of no immediate value for notably mineral exploration purposes, can be of value for precision farming. Furthermore, since readily available, that data carries no extra cost

(*i.e.* no extra flying or remote sensing hardware are required for its acquisition). Such 'collateral information' is illustrated in the next two sections for topographic and environmental parameters of soil.

Land form analysis

During an airborne survey the aircraft positioning is permanently recorded with a DGPS and a laser or radar altimeter. This is done to ensure the aircraft is flying at the right place, elevation and speed against the theoretical flight plan of the survey. The positional information can then in turn be used to establish elevation map of the land being surveyed. The precision of a laser or radar altimeter is certainly not of the caliber of that of a LiDAR survey for example and as such is not suitable enough for terraforming purposes. But with an accuracy of 0.5 to sub-m in x and y and 10-25 cm in z, the information can still be very useful for assessment of the topography (Fig. 10a), slope gradient analysis (Fig. 10b) and ultimately flow patterns analysis of a farm land (not presented here).

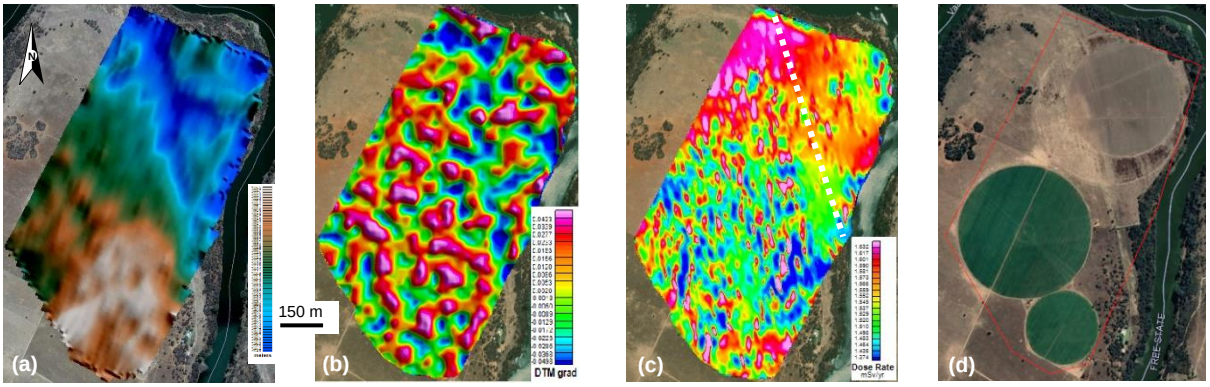

Fig. 10. Land forms and environmental monitoring parameters of the survey area from the airborne geophysical survey. (a) Topographic map established from laser altimeter data (accuracy of ~ 0.5 to 1 in x,y and ~ 10-25 cm in z). (b) Slope gradients map. (c) Radiation dose rate calculated from the radioelements concentration of eK (%), eTh (ppm) and eU (ppm) obtained. White dashed line: position of the underground drain imaged on the Total Magnetic Field map (see Fig. 6). (d) Google Earth image of the study area with footprints of old and newer pivot farms. The red outline corresponds to the airborne survey boundary.

Environmental monitoring parameter

Using the radioelements concentration of eK (%), eTh (ppm) and eU (ppm) obtained from the airborne geophysical survey (see Fig. 3), the radiation dose rate (IAEA, 1991) of the area can be calculated (using expressions from IAEA, 1979, 1991). The dose rate is a measure of the amount of gamma-rays radiation in an area expected to be absorbed by a person. It corresponds only to the terrestrial radiation component and does not include cosmic ray source (impact of which are corrected for as part of the airborne survey data processing) and any other third-party possible radioactive sources (*e.g.* cesium fallout, contaminated irrigation, *etc*). The radiation dose rate map (Fig. 10c) of the study area shows a narrow amplitude of the data ranging from 1.37 to 1.63 µSv yr^{-1}. The northern end of the study area displays the highest level of radiation dose rate. The north-eastern corner of the area shows a far more homogeneous distribution of the radiation dose rate. This is most probably the result of terraforming and/or soil works (tilling) having taken place in that part of the farm land with notably the installation of an underground drainage (white dashed line in Fig 10c – See also Fig. 6 and corresponding text). In the western two thirds of the survey area, there are also a visible N-S and a fainter NW-SE grains or elongations of the highest radiation dose rate anomalies (pink hues in Fig. 10c). This crisscross is not a bias of the airborne survey itself since survey lines were flown NE-SW (see Fig. 3b). It is most probably related to tilling (see marks of tilling in the northern half of the area in the Google Earth image in Fig. 10d) in different directions over time. Interestingly, it seems that the NW-SE direction is more recent as it cuts and also deforms the N-S direction at their intersections. Finally, the radiation dose rate

values in the study area are all above 1 µSv yr^{-1} (Fig. 10c) the value above which the International Commission of Radiological Protection has recommended that no individual should be exposed to. The area is however used for crop farming. The underlying rocks are diabase (Fig. 3c) hence unlikely to be the source of high U and Th from which a dose rate stems from. The high dose rate is instead most probably due to U and Th pollution entering the Mooi River from many existing gold mine slimes dumps in the region and accumulating into its sediments and alluvions, and also possibly through irrigation from the Mooi river.

Conclusions

Light Sport Aircraft aviation have nowadays matured into operational tools providing new horizons compared to conventional aircraft, with lower capital outlay and operational cost as added values. Miniaturization of geophysical technologies lately led to reduction in size, weight and power requirement while increasing sensitivity. With advances in data processing and integration of multiple data streams (here gamma-rays and magnetics), together with support of machine learning and artificial intelligence algorithms (here mainly clustering for soil zones identification), soil conditions mapping can now advance faster and more efficiently than ever before.

Just like in the mineral exploration industry, airborne gamma-rays mapping proves to be a powerful tool for soil mapping. It is successful and fast in predicting, with a resolution at 400 time that of a standard soil sampling program, the content and spatial variability of soil potassium (K), uranium (U) and thorium (Th). It is also successful in predicting soil particle fractions of sand and clay, as well as indirectly (see also Dreyer *et al.*, 2022 – these proceedings) the soil carbon (C), calcium (Ca) and magnesium (Mg).

As expected, separating the magnetic field solely due to the soil from the underlying rock(s) and other influences at depth proved difficult. As a consequence, the calculated soil magnetic susceptibility from the airborne data was not as useful as expected for digital soil mapping. This aspect requires further investigation since magnetics is a critical remote sensing technology that nowadays sustains any natural resources exploration programs (inc. water exploration). Alternative ways to determine the soil magnetic susceptibility through for example the use of both electromagnetic and magnetic techniques should be also considered.

The manipulation of the airborne geophysical data using an integrated approach based on multivariate statistical analysis tools (cluster analyses) enabled data-driven, automated, and rapid data integration as well as value-added digital soil map generation. Further work is however required with respect to calibration aspects of algorithms.

Finally, the airborne geophysical survey also provided extra ancillary information about soil elevation (albeit not to the grade required for terraforming) and environmental (notably the dose rate) parameters with potential to contribute to better decision making on farm land management aspects beyond the sole aspect of digital soil mapping.

Acknowledgments

This paper was supported by EXIGE as part of its airborne agri- & bio-geophysics research and development program. The airborne survey was performed by now defunct GyroLAG Pty Ltd company from South Africa. North West University (South Africa) performed the soil sampling and analyses under le leadership of lecturer and soil scientist J. Dreyer.
The main author wishes to particularly acknowledge the contribution of his collaborator and friend Prof. Marc Munschy (from UNISTRA, France) whom sadly passed away last year. Marc's memory and tremendous scientific and technical contribution to the general development of fluxgate magnetic surveying is a distinct and worthy contribution to the industry and academia.

The authors wish to thank the comments of 3 anonymous reviewers.
In preparation of this paper, the authors have exercised reasonable skill, care and diligence. The statements, conclusions and recommendations might be based upon data and information obtained from third parties. No warranty or undertaking is made in respect of information that was obtained and used in this paper and which, unknown to the authors, was incorrect or incomplete. It is also possible that the authors might have missed certain developments or argument factors, and possibly over or under emphasized others.

References

Améglio, L. (2018). Review of developments in airborne geophysics and geomatics to map variability of soil properties. Proceedings of the 14th *International Conference on Precision Agriculture*, June 24-27, Montreal, Quebec, Canada.

Améglio, L., Durufle, F., Jacobs, G. & Cavern, C. (2015). Light Airborne Platforms for Monitoring Mines and Minerals. 3rd International *Future Mining* conference, Sydney, NSW, 4-6 November.

Beamish D. (2013). Gamma ray attenuation in the soils of Northern Ireland, with special reference to peat. *Journal of Environmental Radioactivity*, 115, 13-27

Beckett, K. (2007). Mapping porosity and density changes in soil and regolith from 256 channel radiometric data. *ASEG,* 2007, Perth, Western Australia.

Beckett, K. (2008). Multispectral processing of high-resolution radiometric data for soil mapping. *Near Surface Geophysics*, 6, 281-287

Bongartz, J.; Weber, I., Jenal, A., Kneer, C., van der Heever, D., Jacobs, G., & Ameglio, L. (2015). Gyrocopter VNIR remote sensing for precision farming. Proceedings of the 14th *SAGA Biennial Technical Meeting and Exhibition*, Drakensberg, South Africa.

Dreyer, J. & Ameglio, L. (2018). The use of aerial gamma-ray spectrometry to determine soil physical and soil chemical properties for soil mapping. Abstract accepted at the 21st World Congress of Soil Science, Brazil, August 2018.

Dreyer, J., van Zijl, G. & Ameglio, L. (2022). Gamma-ray spectrometry to determine soil properties for soil mapping in precision agriculture. Proceedings of the 15th International Conference on Precision Agriculture (unpaginated, online). Monticello, IL: International Society of Precision Agriculture.

Eberle, D., Daudi, E.X.F.G., Muiuane, E.A. & Pontavida, A.M. (2010). Mapeamento aero-geofísico de pegmatitos mineralizados na Província Pegmatítica de Alto Ligonha, no norte de Moçambique. *Revista Brasileira de Geociências*, 40, 527–536.

Egmond van, F., Eddie Loonstra, E., Limburg, H.J., & Minasny, B. (2010). Gamma Ray Sensor for Topsoil Mapping: The Mole. In book: *Proximal Soil Sensing*, pp.323-332.

Foxcroft, N.A. (2019). Studying the relationship between abiotic conditions and nematode pest assemblages in maize. Unpublished. 31 p.

Gustafson, D. E. & Kessel, W. C. (1978). Fuzzy clustering with a fuzzy covariance matrix. Proceedings of the IEEE Conference on *Decision and Control* including the *17th Symposium on Adaptive Processes*, 761–766. doi: 10.1109/CDC.1978.268028.

Horsfall, K.R. (1997). Airborne magnetic and gamma-ray data acquisition. *AGSO Journal of Australian Geology and Geophysics*, 12(2), 23-30.

IAEA – International Atomic Energy Agency (1979). Gamma-raysurveys in uranium exploration. . *Technical Reports Series*, no. 186, IAEA, Vienna, Austria, 90 p.

IAEA – International Atomic Energy Agency (1989). Construction and use of calibration facilities for radiometric field equipment. *Technical Reports Series*, no. 309, IAEA, Vienna, Austria.

IAEA – International Atomic Energy Agency (1991). Airborne gamma-ray spectrometer surveying. IAEA, Vienna, Austria.

IAEA – International Atomic Energy Agency (2003). Guidelines for radio-elements mapping using gamma-ray spectrometry data. IAEA, Vienna, Austria.

Munschy, M., Boulanger, D., Ulrich, P. & Bouiflane, M. (2006). Magnetic mapping for the detection and characterization of UXO: Use of multi-sensor fluxgate 3-axis magnetometers and methods of interpretation. *Journal of Applied Geophysics*, 61, 168-183.

Nazarok, P., Kruglov, O, Menshov, O., Kutsenko, M. & Sukhorada, A. (2014). Mapping soil erosion using magnetic susceptibility. A case study in Ukraine. *Solid Earth Discussion*, 6, 831–848.

Paasche, H. & Eberle, D. (2009). Rapid integration of large airborne geophysical data suites using a fuzzy partitioning cluster algorithm: A tool for geological mapping and mineral exploration targeting: *Exploration Geophysics*, 40, 277–287, doi: 10.1071/EG08028.

Paasche, H. & Eberle, D. (2011). Automated compilation of pseudolithology maps from geophysical data sets: A comparison of Gustafson-Kessel and fuzzy c-means cluster algorithms: *Exploration Geophysics*, 42, 275–285, doi: 10.1071/EG11014.

Reinhardt, N. & Herrmann, L. (2019). Gamma-ray spectrometry as versatile tool in soil science: a critical review. *Journal of Plant. Nutrition and Soil Sciences*, 182, 9-27.

Taylor, M.J., Smethen, K., Pracillo, G. & Verboom, W. (2002). Relationships between soil properties and high-resolution radiometrics, Central Eastern Wheatbelt, Western Australia. *Exploration Geophysics*, 33, 95-102.

Ward, S.H. (1981). Gamma-ray spectrometry in geologic mapping and uranium exploration. *Economic Geology*, 75th Anniversary vol., 840-849.

Wong, M.T.F., Oliver Y.M. & Robertson, M.J. (2007). Gamma-Radiometric Assessment of Soil Depth across a Landscape Not Measurable Using Electromagnetic Surveys. *Journal of Soil Science Society of America*, 73, 1261-1267.